THICKER AND QUICKER: A JUMBO TOKEN FOR FAST PLAIN VISION TRANSFORMERS

Anonymous authors
Paper under double-blind review

ABSTRACT

ViTs are general and accurate, and address many tasks, but ViTs are slow, and are not always practical when efficiency is key. Existing methods for faster ViTs design hybrid non-ViT architectures, losing generality, or shrink their tokens, sacrificing accuracy. While many non-ViT architectures are both fast and accurate, they cannot flexibly process other input shapes, pre-train by SOTA self-supervised learning, reduce computation by dropping tokens, and more like ViTs can. We make ViTs faster by reducing patch token width while *increasing* global token width by adding a new Jumbo token. Our wider Jumbo token is processed by its own wider FFN to increase model capacity. Yet our Jumbo FFN is efficient: it processes a single token, for speed, and its parameters are shared across all layers, for memory. Crucially, our Jumbo is *attention-only* and *non-hierarchical*, like a plain ViT, so it is simple, scalable, flexible, and compatible with ViT methods new and old. Jumbo improves over ViT baselines with Registers from Nano to Large scales *while maintaining speed/throughput* on ImageNet-1K ($\uparrow 0.1-13\%$). Jumbo also improves MAE pre-training ($\uparrow 4.9\%$ linear probing on ImageNet-1K), test-time adaptation ($\uparrow 5.2\%$ on ImageNet-C), and time series modeling. Our Jumbo models even achieve better speed-accuracy trade-offs than *specialized non-ViT* compute-efficient models, while maintaining plain-ViT compatibility for practicality.

1 INTRODUCTION: ARCHITECTURE, ACCURACY, AND EFFICIENCY

For most model sizes, the vision transformer (ViT; Dosovitskiy et al. (2021)) is the go-to architecture in computer vision—powering foundation models like DINOv2 (Oquab et al., 2024), language-aligned models like CLIP (Radford et al., 2021a), segmentation models like SAM (Kirillov et al., 2023), 3D vision models like DUST3R (Wang et al., 2024), and diffusion models like DiT (Peebles & Xie, 2022). These are all "plain" ViTs, which are crucially *attention-only* and *non-hierarchical*.

At the smallest scales—offering the *highest speeds/throughputs*—plain ViTs are not competitive with highly specialized architectures (Yun & Ro, 2024). We attribute the worse accuracy-speed of plain ViTs to their *width* (number of channels). Existing work scales width *equally* across all tokens and layers so higher speed requires lower width: ViT-Base(768)→ViT-Small(384)→ViT-Tiny(192).

We scale width differently across tokens and equally across layers. Our architecture adds a **Jumbo** token, which replaces the conventional `CLS` token, that is $J\times$ wider than the patch tokens, with its own wider feed-forward network (FFN), to effectively and efficiently boost model capacity. For self-attention, the Jumbo token is split into $J\times$ as many tokens/heads, but the Jumbo FFN is only applied to the one (merged) token to reduce time and shared across layers to reduce memory. Jumbo keeps the defining traits of a plain ViT—attention-only and non-hierarchical—so Jumbo applies anywhere a plain ViT does but at higher speed.

The simplicity of ViTs is due to their attention-only and non-hierarchical architecture. Multiple uses of ViTs rely on this architectural "interface" for their computation and function. For instance, this interface enables efficient sparse computation through masking/token dropping. Random token dropping enables efficient training (Liu et al., 2023; Dehghani et al., 2024; Leroy et al., 2024) and learned token dropping enables efficient deployment (Bolya et al., 2023; Fuller et al., 2025). Several SoTA self-supervised learning (SSL) algorithms require token dropping for learning (He et al., 2022; Garrido et al., 2024; Wei et al., 2025; Venkataramanan et al., 2025). This same interface enables flexible processing of different input shapes, like time series (Nie et al., 2023) or video (Arnab et al.,

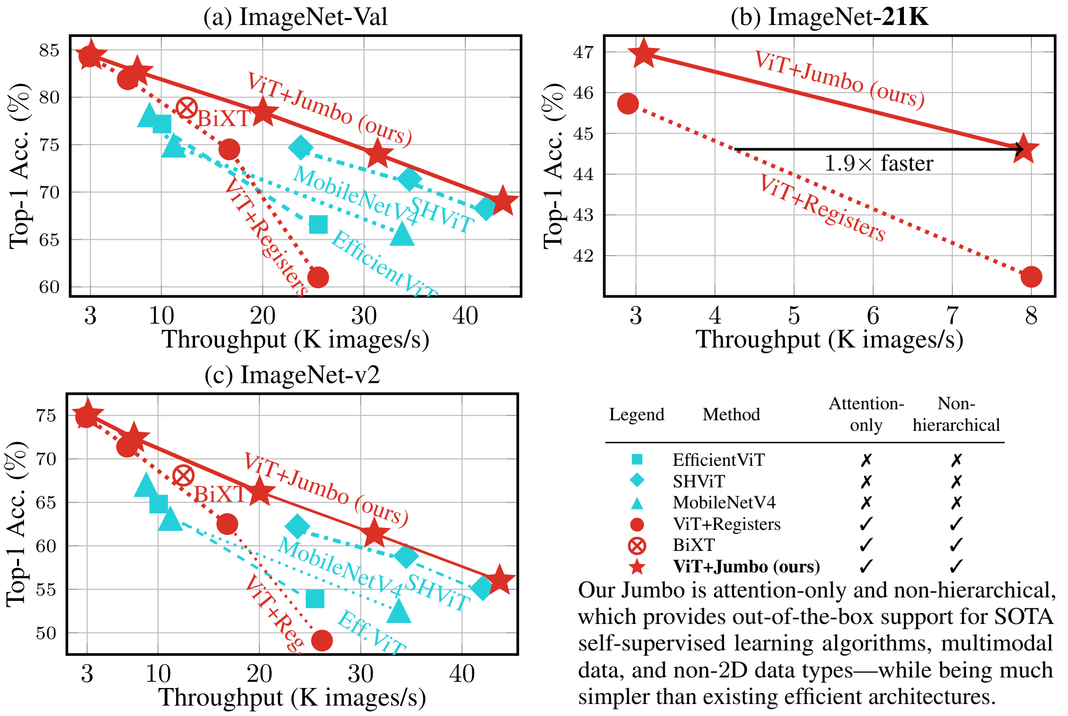

Legend	Method	Attention-only	Non-hierarchical
■	EfficientViT	✗	✗
◆	SHViT	✗	✗
▲	MobileNetV4	✗	✗
●	ViT+Registers	✓	✓
⊗	BiXT	✓	✓
★	**ViT+Jumbo (ours)**	✓	✓

Our Jumbo is attention-only and non-hierarchical, which provides out-of-the-box support for SOTA self-supervised learning algorithms, multimodal data, and non-2D data types—while being much simpler than existing efficient architectures.

Figure 1: Plain ViTs are in red, and others are in blue. ViT+Jumbo outperforms SOTA compute-efficient architectures — *while maintaining the advantages of plain ViTs*. ViT+Jumbo outperforms ViT+Registers on ImageNet-1K and the more challenging ImageNet-21K dataset. Throughput is measured on an RTX 4090 GPU using PyTorch 2.6.0, `torch.compile`, and a 512 batch size.

2021). Moreover, many extensions and applications—from object detection and segmentation heads (Fang et al., 2023; Zhang et al., 2022) to test-time adaptation algorithms (Niu et al., 2023)—are *designed for this plain ViT interface*. Architectures that maintain ViT compatibility inherit all of this.

Our experiments show that Jumbo improves speed-accuracy performance across tasks, datasets, and modalities. ❶ **Image classification**: Jumbo outperforms ViTs by $0.1-13\%$ on ImageNet-1K and $1.2-3.1\%$ on ImageNet-21K *while maintaining throughput* and achieves the pareto frontier vs. compute-efficient architectures. ❷ **Self-Supervised Learning (SSL)**: Jumbo improves MAE (He et al., 2022) pretraining measured with linear probing by 4.9% on ImageNet-1K at ViT-Base scale—this ViT-Base+Jumbo *ties* the ViT-Large baseline, with $2.3\times$ fewer parameters, $3.5\times$ fewer FLOPs, and $3.1\times$ higher throughput. ❸ **Test-time adaptation (TTA)**: Jumbo is more accurate and more robust with 5.2% improvement on ImageNet-C using a SOTA adaptation method for transformers (SAR (Niu et al., 2023)). ❹ **Time series**: Jumbo generalizes beyond vision to rank first across 20 time series benchmarks vs. transformer baselines.

Jumbo is such an efficient ViT-compatible architecture that it outperforms *highly specialized* existing architectures on ImageNet-1K (Fig. 1). This is notable because such compute-efficient architectures (Chen et al., 2023; Howard et al., 2017) sacrifice generality and compatibility with other techniques and applications. Even efficient architectures based on ViTs include convolutions, hierarchy, and batch normalization (Yun & Ro, 2024; Vasu et al., 2023b; Cai et al., 2023) that make them **incompatible** out of the box with SSL by MAE, TTA by SAR, time series, ViT heads, etc. *Jumbo delivers compute efficiency while maintaining plain-ViT compatibility.*

2 Background and Related Work: Generalists and Specialists

2.1 Vision Transformers: Simple, Flexible, but not yet Fast

Jumbo extends ViTs. A ViT splits an image into a patch grid, $\mathbb{R}^{Y\times X\times C}\rightarrow\mathbb{R}^{N_y\times N_x\times P_y\times P_x\times C}$, where C is the number of channels, Y / X are the image height / width, N_y / N_x are the grid height /

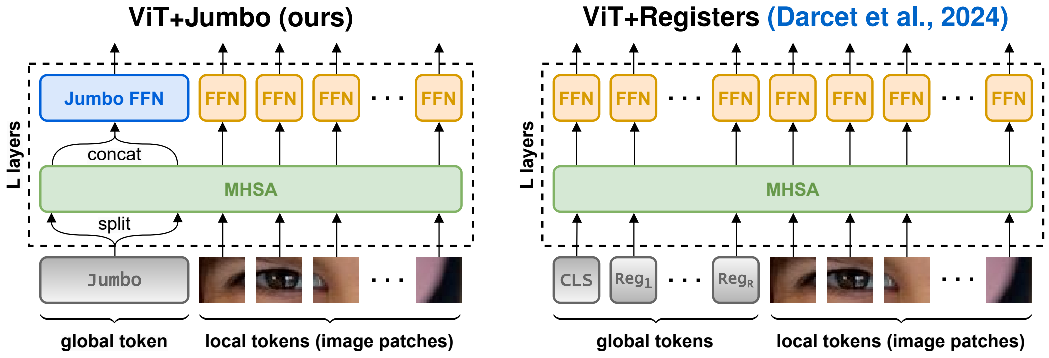

Figure 2: **(Left)** Our ViT+Jumbo method creates a wide global token that gets split into several tokens, with width equal to the patch width, prior to multi-headed self-attention (MHSA). After attention, the split Jumbo token is reassembled via concatenation, and is then processed by ***its own* FFN**. Patches are processed by **their own, shared FFN**. **(Right)** ViT+Registers creates register tokens all equal to the patch width — and all tokens are processed by **a shared FFN**. ViT+Jumbo enhances global processing as the (split) global tokens can interact via an expressive FFN, plus attention.

width, and P_y / P_x are the patch height / width in pixels (equal to $\frac{Y}{N_y}$ / $\frac{X}{N_x}$). Next, they flatten the grid into a sequence and flatten the patches into vectors, $\mathbb{R}^{N_y \times N_x \times P_y \times P_x \times C} \rightarrow \mathbb{R}^{N \times D_{pix}}$, where N is the number of patches (equal to $N_y \cdot N_x$), and D_{pix} is the number of pixel values per patch (equal to $P_y \cdot P_x \cdot C$). Next, they apply a learnable linear projection to form patch embeddings, $\mathbb{R}^{N \times D_{pix}} \rightarrow \mathbb{R}^{N \times D}$, where D is the token width, also known as the embedding dimension. Next, they add position embeddings to patch embeddings. These operations produce patch tokens $\mathbf{x}^P \in \mathbb{R}^{N \times D}$ that represent local information—typically a 16 × 16 px square. Crucially for us, ViTs prepend a learnable `CLS` token $\mathbf{x}^{\texttt{CLS}}$ to the sequence of patch tokens, $\mathbf{x} = \mathbf{x}^{\texttt{CLS}} \|_0 \mathbf{x}^P \in \mathbb{R}^{(N+1) \times D}$, where $\|_0$ denotes concatenation along the 0th (sequence) dimension. Finally, the input $\mathbf{x}$ is processed by a plain transformer and the `CLS` token, having attended to all other tokens, can serve as the global representation of the image. ViT sizes vary w.r.t. depth and width. ViT-Large has 24 layers, others have 12 layers, while the widths vary $\{96,\ 128,\ 192,\ 384,\ 768,\ 1024\}$, corresponding to names {Pico, Nano, Tiny, Small, Base, Large}. Narrower ViTs require less computation and are thus faster.

A standard image size of 224 × 224 px and a standard patch size of 16 × 16 px result in 196 local tokens. A *single* `CLS` token—designed to aggregate global information for classification—provisions 1/197th of a model's representational capacity to global information (and this fraction decreases with larger images and/or smaller patches). This allocation is imbalanced, and may not be optimal. Recent work finds evidence to support this intuition and proposes a fix: register tokens.

Registers. Darcet et al. (2024) find that ViTs learn to repurpose some patch tokens to behave like additional `CLS` tokens by collecting global information and discarding patch-specific local information. The same work proposes a fix: prepend extra learnable tokens—called registers $\mathbf{x}^{\text{Reg}} \in \mathbb{R}^{R \times D}$, where R is the number of registers—to the input sequence, $\mathbf{x} = \mathbf{x}^{\texttt{CLS}} \|_0 \mathbf{x}^{\text{Reg}} \|_0 \mathbf{x}^P \in \mathbb{R}^{(N+R+1) \times D}$. Registers improve accuracy (by ∼0.4% on ImageNet-1K (Russakovsky et al., 2015) at ViT-Base) and reduce attention map artifacts/noise by provisioning more global capacity.

Registers are elegant, simple, and keep the plain ViT interface. In theory, registers can benefit any plain, non-causal transformer. These advantages account for registers' *significant and immediate* impact including in applications beyond images (Dong et al., 2024; Vaquero et al., 2024; Leigh et al., 2024; Messaoud et al., 2025; Hu et al., 2024; Thimonier et al., 2024; Omranpour et al., 2024). Our Jumbo is inspired by ViT+Registers: see Fig. 2 for their relationship and key differences.

2.2 Compute-efficient Architectures: Fast, but not Simple nor Flexible

The Jumbo architecture is accurate and compute-efficient, so we highlight 3 architectures and use them as baselines for high-speed ViTs. ❶ EfficientViT (Cai et al., 2023) and ❷ SHViT (Yun & Ro, 2024) improve the efficiency of ViTs by incorporating efficient attention, pooling, and convolutional layers. ❸ MobileNetV4 (Qin et al., 2025) improves the efficiency of CNNs by leveraging many strategies (and different strategies for different model sizes). These baselines represent the SOTA in computational efficiency; please refer to Appendix A.2 for descriptions of these model architectures.

Beyond these, there is a rich literature on compute-efficient vision architectures. For example, several efficient CNN-based architectures exist (Howard, 2017; Sandler et al., 2018; Howard et al., 2019; Han et al., 2020; Tan et al., 2019; Vasu et al., 2023a); however, these are surpassed by MobileNetV4 (Qin et al., 2025). Since the invention of the ViT, there have been many compute-efficient "ViTs" that incorporate efficiencies inspired by CNN-based approaches (Vasu et al., 2023b; Mehta & Rastegari, 2021; 2022; Li et al., 2023; Pan et al., 2022; Chen et al., 2022; Li et al., 2022). SHViT (Yun & Ro, 2024) has recently surpassed these architectures. Despite their impact and ingenuity, none of these hybrid architectures meets the definition of a plain ViT, which is attention-only and non-hierarchical; they thus lose many advantages of ViTs that we wish to keep. On the other hand, BiXT (Hiller et al., 2024) models are an efficient extension of the Perceiver architecture (Jaegle et al., 2021) that keeps the attention-only and non-hierarchical properties of ViTs, which are a natural comparison to Jumbo.

3 Method: A Jumbo token for a Compute-Efficient Plain ViT

3.1 Design Motivation and Intuition

Capacity and Cost. Although Jumbo adds a wider token and FFN, the cost is minimal. *The key insight is that a single wide token affords much greater width and more processing without slower speed.* As shown in Fig. 3, the main drivers of computational cost (FLOPs per layer) are sequence length and patch width, D. The FLOP contribution from our Jumbo token is comparatively negligible. Since our architecture shares Jumbo FFN parameters across all ViT layers, its memory costs are also minimal.

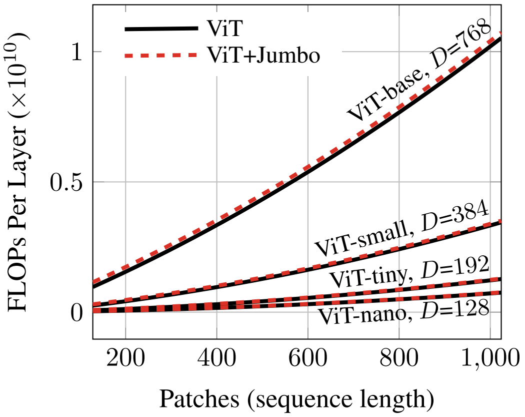

Figure 3: The cost of layers is largely determined by the number of patches and their width D. The cost of our Jumbo token (J=6) is negligible.

Non-hierarchical and attention-only. Jumbo preserves the non-hierarchical shape of ViTs (also known as columnar or isotropic shape). By foregoing convolutions, spatial information only moves through attention. These two properties have several advantages that we now discuss.

Token Dropping / Masking. Although convolutions are capable of processing a sparse subset of patches via sparse compute kernels, these kernels can be complex, challenging to use, and require updating when new hardware arrives. Furthermore, sparse convolutional kernels will never be as efficient as simply indexing from a sequence—i.e., how transformers drop tokens. As a comparison, ConvNeXt V2 (Woo et al., 2023) reports a 1.3× speedup using a 60% masking ratio with the Minkowski Engine v0.5.4 (Choy et al., 2019). Conversely, MAE (He et al., 2022) report $2.8 - 4.1\times$ speedups using a 75% masking ratio with plain ViTs. *Efficient token dropping is required for SOTA SSL algorithms* (Assran et al., 2023; Fu et al., 2024; Garrido et al., 2024; Wei et al., 2025; Venkataramanan et al., 2025; Oquab et al., 2024). Token dropping also speeds up supervised training (Dehghani et al., 2024). We demonstrate Jumbo's token dropping ability in subsections 4.2 and 4.4.

Other Data Modalities and Shapes. These properties explain the input flexibility of transformers, which Jumbo keeps. For example, 1D time series, 3D point clouds, or multimodal data; users need only adjust tokenization strategies. We show a 1D time series application of Jumbo in subsection 4.5.

Plain ViT's Ecosystem. These two properties—non-hierarchical and attention-only—maintain support for methods invented for the plain ViT. For example, segmentation and object detection heads (Fang et al., 2023; Liu et al., 2025; Zhang et al., 2022), which expect ViT's unpooled feature map; test-time adaptation methods (Niu et al., 2023), designed for the LayerNorm (Ba et al., 2016) *not* BatchNorm (Ioffe & Szegedy, 2015); and attention improvements, such as Flash Attention (Dao et al., 2022), which can speed up self-attention by $> 5\times$. *Jumbo supports these innovations out of the box.*

Crucially, *none* of the compute-efficient architectures in subsection 2.2 immediately benefit from these advances, support other data modalities or token dropping, or integrate with the ViT ecosystem.

Two hypotheses. Jumbo asymmetrically increases the model capacity. Thus, ❶ we expect increasing gains due to Jumbo with *decreasing* patch token width. ❷ We expect increasing gains due to Jumbo with *increasing* task output dimensionality. We explore both of these hypotheses using experiments with ViTs of different widths and datasets of different complexities.

3.2 Design Specifics for Token-Width Asymmetry

Exactly like the original ViT, Jumbo computes patch embeddings, $\mathbf{x}^P \in \mathbb{R}^{N \times D}$. Unlike the original ViT, our method creates a Jumbo token that is J times wider than the patch width D, $\mathbf{x}^{\texttt{Jumbo}} \in \mathbb{R}^{J \cdot D}$. Architecturally identical transformer layers then process these inputs.

Before self-attention, the Jumbo token is split into J tokens, $|_J^1 \ \mathbf{x}^{\texttt{Jumbo}} : \mathbb{R}^{1 \times J \cdot D} \rightarrow \mathbb{R}^{J \times D}$, where $|_J^1$ denotes splitting into J segments along the 1st (feature) dimension. Next, the split Jumbo token is concatenated with patch embeddings along the sequence dimension, $\mathbf{x} = \mathbf{x}^{\texttt{Jumbo}} \|_0 \mathbf{x}^P \in \mathbb{R}^{(N+J) \times D}$. This sequence is sent through a plain multi-headed self-attention layer. Afterward, the Jumbo token is extracted from the sequence by splitting along the sequence dimension, $|_2^0 \ \mathbf{x} : \mathbb{R}^{(N+J) \times D} \rightarrow (\mathbb{R}^{J \times D}, \mathbb{R}^{N \times D})$, where the first element contains the (still split) Jumbo token and the second element contains the patch representations. Finally, the Jumbo token is reassembled through concatenation along the channel dimension, $\mathbf{x}^{\texttt{Jumbo}} = \|_1 \mathbf{x}^{\texttt{Jumbo}} : \mathbb{R}^{J \times D} \rightarrow \mathbb{R}^{1 \times J \cdot D}$. These two splits and two concatenations add negligible runtime overhead.

After self-attention, the Jumbo token is processed by its own FFN that does not share parameters with the patch FFN. Fig. 2 indicates this by coloring the Jumbo and patch FFNs differently. After processing by all layers, we project the Jumbo token to C class logits, $\mathbb{R}^{J \cdot D} \rightarrow \mathbb{R}^C$.

Layer sharing. We share our Jumbo FFN parameters across all layers to reduce memory use (through fewer model parameters). All other model parameters are not shared across layers, as usual. Sharing also acts as regularization. Empirically, we find sharing keeps (and sometimes increases) Jumbo's accuracy gains compared with *not* layer sharing—while effectively controlling memory use. Sharing the FFN layer is thus the default in our Jumbo architecture.

4 Experiments: Accuracy, Compute Efficiency, and Generality

For all experiments, we measure throughput on an RTX 4090 GPU using PyTorch 2.6.0, `torch.compile`, and a 512 batch size.

4.1 ImageNet-1K Experiments with Compute-Efficient Baselines

Setup. We perform controlled experiments to evaluate Jumbo. Specifically, we train models from scratch on ImageNet-1K (Russakovsky et al., 2015) at 128×128 px for 400 epochs, then for 20 epochs at 224×224 px. We leverage distillation to improve convergence, which is a common strategy.

We train each model architecture twice, once for each learning rate $\{1\text{e}{-}3, 3\text{e}{-}3\}$ (Touvron et al., 2022; Yun & Ro, 2024) using a 1024 batch size with the AdamW optimizer (Loshchilov, 2017). We report the results of the best learning rate for each model architecture. Please see Appendix A.3.1 & A.4 for hyperparameters and complete results, respectively.

Baselines. We choose the high-speed models for each family: ❶ ViT+Registers {Nano, Tiny, Small, Base} (Darcet et al., 2024), ❷ BiXT has 1 size (tiny), ❸ EfficientViT {B0, B1} (Cai et al., 2023), ❹ SHViT {S1, S2, S3} (Yun & Ro, 2024), and ❺ MobileNetV4 {Conv-Small, Conv-Medium, Hybrid-Medium} (Qin et al., 2025). We compare these architectures with our high-speed ViT+Jumbo variants {Pico, Nano, Tiny, Small, Base}. Darcet et al. (Darcet et al., 2024) show ViT+Registers with R=16 performs best, which we confirm in the appendix Table 7 and use in these experiments. We show ViT+Jumbo is robust to the choice of J; we use J=6 and study its effect in the appendix Table 12.

Test Sets. We test all models on the three most common ImageNet-1K test sets: ImageNet-Val (Russakovsky et al., 2015), ImageNet-ReaL (Beyer et al., 2020), and ImageNet-v2 (Recht et al., 2019). To further evaluate generalization we also test all models on ImageNet-HR (Fuller et al.,

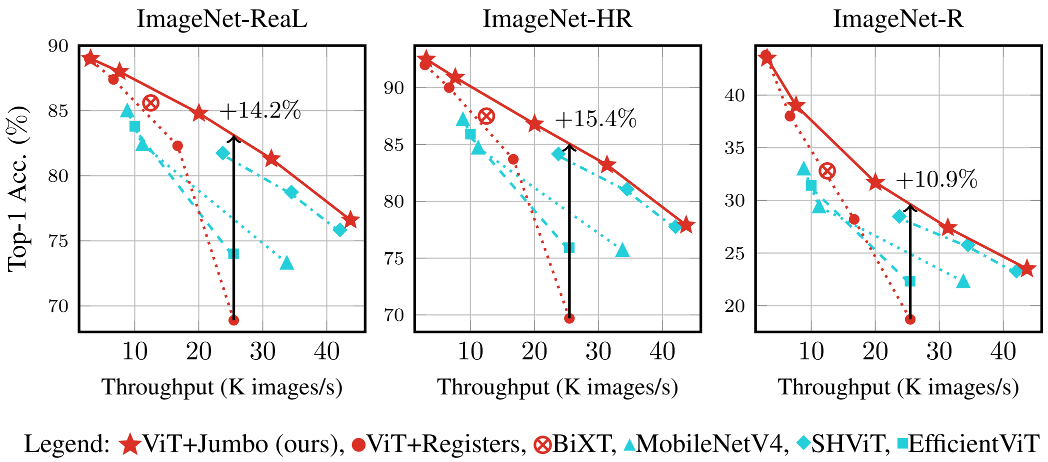

Figure 4: ViT+Jumbo achieves the Pareto frontier and is much simpler than specialized compute-efficient architectures. Results are plotted for each model's best learning rate. Throughput is measured on an RTX 4090 GPU using PyTorch 2.6.0, `torch.compile`, and a 512 batch size.

2024), for its image diversity and high-quality annotations, ImageNet-R (Hendrycks et al., 2021), for its out-of-distribution images.

Results. As illustrated in Fig 4, Jumbo achieves the Pareto frontier on ImageNet-1K. Crucially, Jumbo achieves these results while preserving the many advantages and simplicity of plain ViTs. Even matching the specialized compute-efficient architectures makes a strong case for ViT+Jumbo.

ViT+Jumbo outperforms ViT+Registers by 13% at the nano scale and 4% at the tiny scale, where such gains are significant. This confirms our first hypothesis that Jumbo's gains should increase as we decrease the patch width, i.e., from Small (384) to Tiny (192) to Nano (128) (Figs. 1a, 4).

ViT+Jumbo is a clear choice if a researcher or practitioner requires high speed and out-of-the-box ViT compatibility for SSL algorithms or multimodal processing. ViT+Registers is not as accurate at high speed, while the specialized compute-efficient architectures do not support most SOTA SSL algorithms or flexible processing across modalities. Remote sensing (Rolf et al., 2024) and autonomous driving (Muhammad et al., 2020) are two of many applications where this combination of speed, SSL support, and multimodal processing is particularly valuable.

4.2 ImageNet-21K Experiments with ViT Comparisons

ImageNet-1K is a subset of the more challenging, original ImageNet (Deng et al., 2009), now referred to as ImageNet-21K. We use a common variant comprising 10,450 classes that includes processing to make a more accessible benchmark (Ridnik et al., 2021). This dataset provides more than 10× the number of classes and samples as ImageNet-1K, making it well suited to test our second hypothesis—that is, gains due to Jumbo should increase with increasing task-output dimensionality.

Setup. We train models from scratch on ImageNet-21K. Since training models on ImageNet-21K is expensive, we leverage a token dropping strategy to reduce costs. Specifically, we start training with a 90% token drop rate and linearly decrease this value to 10%; this halves the total number of tokens processed. Dehghani et al. (2024) demonstrate the effectiveness of this strategy, i.e., leveraging "masking" with plain supervised training. Plain ViTs support masking with minimal code changes. We train each model architecture once, for 50 epochs using a 3e$-$3 learning rate and a 1024 batch size with the AdamW optimizer (Loshchilov, 2017) (see the Appendix A.3.1 for other hyperparameters).

Baselines. We choose ViT+Registers {Small, Base} to compare with our ViT+Jumbo {Small, Base} sizes. This is a more narrow but valid comparison, as the plain ViT is the vision community's preferred architecture at these scales. For ViT+Registers, we use R=16; for ViT+Jumbo, we use J=6 for the Small model and J=3 for the Base model.

Results. ViT+Jumbo outperforms ViT+Registers by 3.1% and 1.2% at ViT-Small and ViT-Base scales, respectively (see Fig. 1b). Gains due to Jumbo increase when scaling from ImageNet-1K to ImageNet-21K for a given model size, e.g., ViT-Small gains increase from 0.8% (Fig. 1a) to 3.1%. Thus, these findings confirm our second hypothesis that gains due to Jumbo should increase with increasing output dimensionality. Furthermore, for a given accuracy Jumbo is 1.9× faster (Fig. 1b).

4.3 Masked Autoencoding Experiments

Setup. We pretrain Jumbo ViT-Base and ViT-Large models using masked autoencoding (MAE; (He et al., 2022)) using the default settings. This tests Jumbo's ability in a standard SSL framework. This also tests Jumbo's scalability to larger models (up to ViT-Large) and longer training schedules (up to 1600 epochs on ImageNet-1K). These experiments are expensive, so we leverage free TPU resources, perform no hyperparameter tuning, and compare against plain ViT results obtained with the same MAE implementation. After pretraining, we linear probe on ImageNet-1K to obtain accuracies.

Table 1: **MAE Pretraining.** Jumbo significantly outperforms standard ViT. Jumbo scales to these large MAE models and their long training schedules (1600 epochs for ViT-Base, 800 epochs for ViT-Large). After pretraining, we linearly probe to compute top-1 accuracy on ImageNet-1K.

Architecture	Speed	Params	Memory	FLOPs	Top-1 Acc.
	K imgs/s	M	GB	G	%
ViT-base	3.1	86.6	3.3	16.5	68.1
ViT-base+Jumbo	3.1	130.7	3.9	16.9	**73.0**
ViT-large	1.0	304.4	5.0	59.7	73.0
ViT-large+Jumbo	1.0	382.2	5.2	59.9	**74.0**

Results. Our ViT-Base+Jumbo MAE outperforms the baseline by 4.9% on ImageNet-1K. ViT-**Base**+Jumbo *ties* the ViT-**Large** MAE, while Jumbo is 3× faster with only 0.43× the parameters. This shows Jumbo can be applied to SSL by MAE to improve performance without further modification. The role of masking in the MAE suggests that the wider Jumbo token stores more global information. For this MAE, Jumbo is a more efficient way to scale model parameters than the wider ViT.

4.4 Robustness and Test-Time Adaptation Experiments

Setup. We measure robustness to corruption with and without adaptation. We follow SAR (Niu et al., 2023) exactly, swapping in ViT-S models with Registers or our Jumbo from Sec. 4.1, and measure robustness to 15 corruptions at the highest severity from ImageNet-C (Hendrycks & Dietterich, 2019).

Table 2: **Test-Time Adaptation (TTA).** Jumbo improves plain-ViT robustness *without* TTA (avg. ↑3.6%) and *with* TTA (avg. ↑5.2%) on ImageNet-C. We follow SAR (Niu et al., 2023) and test across 15 shifts at the highest severity. Jumbo is directly compatible with SOTA methods designed for ViTs, for instant use without tuning, unlike highly-specialized architectures (MobileNet, SHViT, ...).

Method	Gauss.	Shot	Impul.	Defoc.	Glass	Motion	Zoom	Snow	Frost	Fog	Brit.	Contr.	Elastic	Pixel	JPEG	Avg.
Registers	13.6	14.2	13.0	29.3	20.3	34.9	28.7	49.0	50.4	56.6	73.5	47.8	29.0	45.6	56.1	37.5
Jumbo	**25.9**	**26.6**	**25.8**	**31.2**	**21.4**	**33.3**	**30.6**	**53.1**	**51.9**	**57.3**	**75.2**	**49.4**	**30.5**	**47.5**	**57.1**	**41.1**
Registers+SAR	38.9	39.2	41.5	48.2	48.7	56.5	32.1	62.0	59.4	68.9	76.1	61.5	59.1	65.5	66.1	54.9
Jumbo+SAR	**45.2**	**49.6**	**51.2**	**53.3**	**53.2**	**61.1**	**44.5**	**66.2**	**58.5**	**71.7**	**77.5**	**67.1**	**65.2**	**69.0**	**69.0**	**60.1**

Results. Jumbo is both more accurate than Registers (+0.8% on IN-Val) and more robust than Registers on corrupted data (+3.6% on IN-C). Test-time adaptation by SAR further increases the robustness gain to +5.2%. In principle test-time adaptation can apply to any architecture, but in practice methods specialize. SOTA methods such as SAR are designed for the plain ViT LayerNorm, and not the BatchNorm of SHViT, MobileNetV4, and EfficientViT, so ViT compatibility is a plus.

4.5 Time Series Experiments

Jumbo can easily process different input shapes (beyond images) because it maintains the plain transformer interface. We apply Jumbo to time series inputs. PatchTST (Nie et al., 2023) is a SOTA patch-based transformer for time series that we extend with registers (PatchTST+Registers) or Jumbo (PatchTST+Jumbo).

Setup. We train models from scratch on ❶ 10 univariate time series datasets from the UCR archive (Dau et al., 2018), and ❷ 10 multivariate time series datasets from the UEA archive (Bagnall et al., 2018); both of which are commonly used benchmarks (Zerveas et al., 2021; Grover et al., 2024; Le et al., 2024). For each dataset and model, we perform a hyperparameter sweep from the Cartesian product of learning rate $\{3e{-}3, 1e{-}3, 3e{-}4, 1e{-}4\}$, and dropout $\{0.0, 0.1, 0.2\}$. More details are in Appendix A.3.2. We report the best run and the average of all 12 runs per experiment in the appendix Tables 13 & 14. To summarize these results, we compute the rank between models and then average the ranks over the 10 univariate and 10 multivariate datasets.

Baselines. We compare PatchTST with our PatchTST+Jumbo method and our PatchTST+Registers baseline. We experiment with 8 and 42 patches per sequence for all three models. Jumbo and registers are both simple to adopt for PatchTST because they remain plain transformers.

Table 3: **Time series** rankings using PatchTST (Nie et al., 2023) with Registers or Jumbo (*lower is better* and the best is in bold). We rank over 10 univariate and 10 multivariate datasets. "Best" is the best run of our 12-run hyperparameter sweep and "Avg" is the average over the sweep. Jumbo achieves the best ranking in all experiments. We use two patch sizes: 8/42 (results are formatted likewise).

		PatchTST	PatchTST +Registers	PatchTST +Jumbo
Univar.	Best	2.0/1.9	2.5/2.1	**1.5/1.7**
	Avg	2.9/2.3	2.1/2.4	**1.0/1.3**
Multivar.	Best	2.1/2.0	2.1/1.9	**1.6/1.7**
	Avg	2.7/2.6	2.0/2.4	**1.3/1.0**

Results. PatchTST+Jumbo outperforms strong PatchTST and PatchTST+Registers baselines (Tab. 3). Jumbo gains the most with fewer patches and when considering overall results across hyperparameters. These results establish that Jumbo can improve non-causal transformers beyond ViTs.

4.6 Ablations

Table 4: Jumbo's shared FFN increases accuracy and is memory efficient. Our Jumbo FFN can be enlarged ($J{=}10$) for even higher performance, at relatively low cost. We report top-1 accuracy on ImageNet-21K.

Architecture	Speed K imgs/s ↑	Params M	Memory GB ↓	FLOPs G ↓	Top-1 Acc. % ↑
Jumbo (Fig. 1b)	7.9	88.3	2.6	4.6	44.61
Jumbo without layer sharing	7.7	555.6	4.1	4.6	44.95
Jumbo without Jumbo FFN	8.4	45.8	2.2	4.4	43.64
Jumbo with LoRA, rank=8	7.7	88.8	2.5	4.6	44.94
Jumbo J: 6→10	6.9	179.9	3.4	5.5	45.62

Setup. We follow our ImageNet-21K training recipe and ablate Jumbo's design at ViT-Small scale to better understand the contributions of the architecture and its design choices.

Results. (Tab. 4) Not sharing the Jumbo FFN across layers slightly improves accuracy at this scale. However, we can fully recover from the drop with sharing by adapting the Jumbo FFN parameters with LoRAs (Hu et al., 2022): we still share the Jumbo FFN across layers but apply layer-specific LoRAs to specialize efficiently. LoRAs recover accuracy at negligible cost in speed and memory. Jumbo without Jumbo FFNs performs well enough (2.2% better than ViT+Registers) but worse than Jumbo: the main difference between this ablation and ViT+Registers is that it concatenates all global tokens as input to the classifier (rather than discarding registers). Yet, our best ViT-Small includes the Jumbo FFN: with $J{=}10$ its shared FFN achieves 45.6% top-1 accuracy. This Jumbo model beats ViT-Small+Registers by 4.1% and matches ViT-**Base**+Registers (0.1% difference) with higher speed (2.4× faster) and less memory.

4.7 Analysis: How to Scale Efficiency and Capacity

Is Jumbo more accurate just because it has more parameters? No. We take ViT-B+Registers and increase its width $768{\to}1024$ to equalize the number of parameters with our ViT-Base+Jumbo (Tab. 5 rows 1 & 3). These models differ in accuracy by 0.1%,

Table 5: ViT-Base+Jumbo matches a *symmetrically wider* ViT+Registers with equal params; yet our Jumbo is 1.7× faster. Jumbo also outperforms other ways of adding global capacity, e.g., ❶ uses an FFN for patches, and a separate FFN for CLS+Reg. tokens, ❷ uses an FFN for patches+CLS, and separate FFN for Reg. tokens. We report top-1 accuracy on ImageNet-21K.

Architecture	Speed K imgs/s ↑	Params M	Memory GB ↓	FLOPs G ↓	Top-1 Acc. % ↑
ViT-Base models					
Jumbo	3.1	152.5	4.1	16.5	46.95
Reg. (Darcet et al., 2024)	2.9	93.9	3.5	18.2	45.73
Registers D: 768→1024	1.8	162.9	4.5	32.4	47.08
ViT-Small models					
Jumbo	7.9	88.3	2.6	4.6	44.61
Reg. (Darcet et al., 2024)	8.0	25.7	2.3	4.6	41.48
Alt. ❶: CLS+Reg. FFN	7.7	39.9	2.3	4.6	41.51
Alt. ❷: Reg. FFN	7.7	39.9	2.3	4.6	42.11

yet Jumbo is more efficient with 1.7× the throughput, 0.5× the FLOPs, and 0.9× the memory. Our novel asymmetric-width design of the Jumbo token and FFN is crucial to its better efficiency.

Alternate ViT+Register designs. We experiment with two more architectures to investigate the role of adding separate FFNs for different types of tokens (Tab. 5). Alternative ❶ has an FFN for all patch tokens with a *separate* FFN for the CLS and registers. Alternative ❷ has an FFN for all patch tokens *and* the CLS token with a separate FFN for the registers. Neither model gains much: the asymmetric token width of Jumbo explains its success, and *not* the addition of more parameters alone.

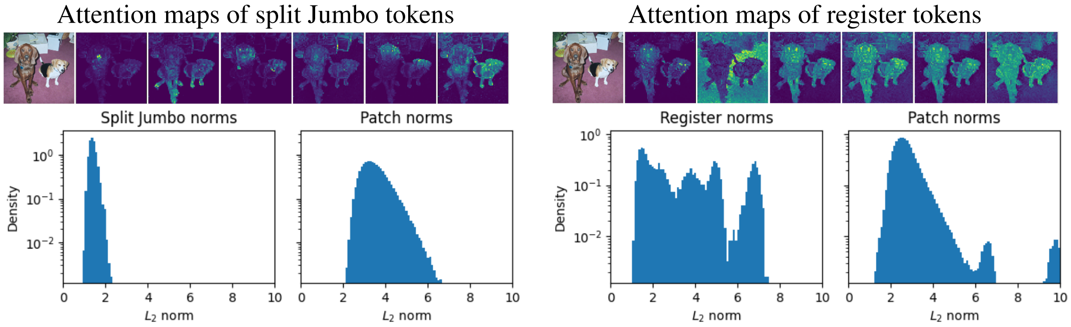

Figure 5: Jumbo (left two subfigures) eliminates high-norm, outlier tokens in our measurements. According to Darcet et al. (Darcet et al., 2024), outlier tokens cause attention-map artifacts, and their presence can be reduced by adding registers (right two subfigures). By inspection, Jumbo also learns artifact-free attention maps, and split Jumbo tokens seem to specialize.

Does Jumbo also reduce high-norm tokens? Registers reduce high-norm, outlier tokens that cause attention map artifacts (Darcet et al., 2024). We test if Jumbo does the same. The ViT+Jumbo models we train are in fact *more effective* at reducing outlier tokens than ViT+Registers (Fig. 5). We also show attention maps in the Appendix A.6 where we again see a similar effect.

5 Discussion: Efficiency, Generality, and Capacity

Limitations and Future Work. In this work, we do not evaluate Jumbo in vision-language (e.g., CLIP (Radford et al., 2021b)) or language-only applications (e.g., BERT (Devlin et al., 2019), which is non-causal and could benefit from Jumbo in theory). We save these applications for future work.

Conclusion. Jumbo is highly efficient, simple, and general: our Jumbo ViTs achieve SOTA accuracy-speed trade-offs by a targeted increase in the global computation and parameter capacity of any plain ViT. We show that upgrading a plain ViT with Jumbo improves accuracy at the same speed or maintains accuracy at faster speeds for supervised image classification, self-supervised learning, time series modeling, and test-time adaptation. Jumbo is the first attention-only and non-hierarchical architecture to outperform specialized compute-efficient architectures like EfficientViT (Cai et al., 2023). To do so Jumbo increases width *asymmetrically*, across tokens, and not across layers (in contrast to existing hierarchical models). While increasing model capacity can increase accuracy, it is critical to add capacity in the right places to *achieve high efficiency and maintain model flexibility* as we show with Jumbo.

REFERENCES

Anurag Arnab, Mostafa Dehghani, Georg Heigold, Chen Sun, Mario Lucic, and Cordelia Schmid. ViViT: A Video Vision Transformer . In *2021 IEEE/CVF International Conference on Computer Vision (ICCV)*, 2021. doi: 10.1109/ICCV48922.2021.00676.

Mahmoud Assran, Quentin Duval, Ishan Misra, Piotr Bojanowski, Pascal Vincent, Michael Rabbat, Yann LeCun, and Nicolas Ballas. Self-supervised learning from images with a joint-embedding predictive architecture. In *Proceedings of the IEEE/CVF Conference on Computer Vision and Pattern Recognition*, pp. 15619–15629, 2023.

Jimmy Lei Ba, Jamie Ryan Kiros, and Geoffrey E. Hinton. Layer normalization, 2016. URL `https://arxiv.org/abs/1607.06450`.

Anthony Bagnall, Hoang Anh Dau, Jason Lines, Michael Flynn, James Large, Aaron Bostrom, Paul Southam, and Eamonn Keogh. The uea multivariate time series classification archive, 2018. URL `https://arxiv.org/abs/1811.00075`.

Lucas Beyer, Olivier J Hénaff, Alexander Kolesnikov, Xiaohua Zhai, and Aäron van den Oord. Are we done with imagenet? *arXiv preprint arXiv:2006.07159*, 2020.

Lucas Beyer, Xiaohua Zhai, Amélie Royer, Larisa Markeeva, Rohan Anil, and Alexander Kolesnikov. Knowledge distillation: A good teacher is patient and consistent. In *Proceedings of the IEEE/CVF conference on computer vision and pattern recognition*, pp. 10925–10934, 2022.

Daniel Bolya, Cheng-Yang Fu, Xiaoliang Dai, Peizhao Zhang, Christoph Feichtenhofer, and Judy Hoffman. Token merging: Your vit but faster. In *The Eleventh International Conference on Learning Representations*, 2023. URL `https://openreview.net/forum?id=JroZRaRw7Eu`.

Han Cai, Junyan Li, Muyan Hu, Chuang Gan, and Song Han. Efficientvit: Lightweight multi-scale attention for high-resolution dense prediction. In *Proceedings of the IEEE/CVF International Conference on Computer Vision*, pp. 17302–17313, 2023.

Jierun Chen, Shiu-hong Kao, Hao He, Weipeng Zhuo, Song Wen, Chul-Ho Lee, and S-H Gary Chan. Run, don't walk: chasing higher flops for faster neural networks. In *Proceedings of the IEEE/CVF conference on computer vision and pattern recognition*, pp. 12021–12031, 2023.

Yinpeng Chen, Xiyang Dai, Dongdong Chen, Mengchen Liu, Xiaoyi Dong, Lu Yuan, and Zicheng Liu. Mobile-former: Bridging mobilenet and transformer. In *Proceedings of the IEEE/CVF conference on computer vision and pattern recognition*, pp. 5270–5279, 2022.

Christopher Choy, JunYoung Gwak, and Silvio Savarese. 4d spatio-temporal convnets: Minkowski convolutional neural networks. In *Proceedings of the IEEE/CVF conference on computer vision and pattern recognition*, pp. 3075–3084, 2019.

Ekin D Cubuk, Barret Zoph, Dandelion Mane, Vijay Vasudevan, and Quoc V Le. Autoaugment: Learning augmentation policies from data. *arXiv preprint arXiv:1805.09501*, 2018.

Tri Dao, Dan Fu, Stefano Ermon, Atri Rudra, and Christopher Ré. Flashattention: Fast and memory-efficient exact attention with io-awareness. *Advances in Neural Information Processing Systems*, 35:16344–16359, 2022.

Timothée Darcet, Maxime Oquab, Julien Mairal, and Piotr Bojanowski. Vision transformers need registers. In *The Twelfth International Conference on Learning Representations*, 2024. URL `https://openreview.net/forum?id=2dnO3LLiJ1`.

Hoang Anh Dau, Anthony J. Bagnall, Kaveh Kamgar, Chin-Chia Michael Yeh, Yan Zhu, Shaghayegh Gharghabi, Chotirat Ann Ratanamahatana, and Eamonn J. Keogh. The UCR time series archive. *arXiv preprint arXiv:1810.07758*, 2018.

Mostafa Dehghani, Basil Mustafa, Josip Djolonga, Jonathan Heek, Matthias Minderer, Mathilde Caron, Andreas Steiner, Joan Puigcerver, Robert Geirhos, Ibrahim M Alabdulmohsin, et al. Patch n'pack: Navit, a vision transformer for any aspect ratio and resolution. *Advances in Neural Information Processing Systems*, 36, 2024.

Jia Deng, Wei Dong, Richard Socher, Li-Jia Li, Kai Li, and Li Fei-Fei. Imagenet: A large-scale hierarchical image database. In *2009 IEEE conference on computer vision and pattern recognition*, pp. 248–255. Ieee, 2009.

Jacob Devlin, Ming-Wei Chang, Kenton Lee, and Kristina Toutanova. Bert: Pre-training of deep bidirectional transformers for language understanding. In *Proceedings of the 2019 conference of the North American chapter of the association for computational linguistics: human language technologies, volume 1 (long and short papers)*, pp. 4171–4186, 2019.

Xin Dong, Yonggan Fu, Shizhe Diao, Wonmin Byeon, Zijia Chen, Ameya Sunil Mahabaleshwarkar, Shih-Yang Liu, Matthijs Van Keirsbilck, Min-Hung Chen, Yoshi Suhara, Yingyan Lin, Jan Kautz, and Pavlo Molchanov. Hymba: A hybrid-head architecture for small language models, 2024. URL `https://arxiv.org/abs/2411.13676`.

Alexey Dosovitskiy, Lucas Beyer, Alexander Kolesnikov, Dirk Weissenborn, Xiaohua Zhai, Thomas Unterthiner, Mostafa Dehghani, Matthias Minderer, Georg Heigold, Sylvain Gelly, Jakob Uszkoreit, and Neil Houlsby. An image is worth 16x16 words: Transformers for image recognition at scale. In *International Conference on Learning Representations*, 2021. URL `https://openreview.net/forum?id=YicbFdNTTy`.

Yuxin Fang, Shusheng Yang, Shijie Wang, Yixiao Ge, Ying Shan, and Xinggang Wang. Unleashing vanilla vision transformer with masked image modeling for object detection. In *Proceedings of the IEEE/CVF International Conference on Computer Vision*, pp. 6244–6253, 2023.

Letian Fu, Long Lian, Renhao Wang, Baifeng Shi, Xudong Wang, Adam Yala, Trevor Darrell, Alexei A. Efros, and Ken Goldberg. Rethinking patch dependence for masked autoencoders. *arXiv preprint arXiv:2401.14391*, 2024.

Anthony Fuller, Daniel Kyrollos, Yousef Yassin, and James R Green. Lookhere: Vision transformers with directed attention generalize and extrapolate. In *The Thirty-eighth Annual Conference on Neural Information Processing Systems*, 2024. URL `https://openreview.net/forum?id=o7DOGbZeyP`.

Anthony Fuller, Yousef Yassin, Junfeng Wen, Daniel G. Kyrollos, Tarek Ibrahim, James R. Green, and Evan Shelhamer. Lookwhere? efficient visual recognition by learning where to look and what to see from self-supervision, 2025. URL `https://arxiv.org/abs/2505.18051`.

Quentin Garrido, Mahmoud Assran, Nicolas Ballas, Adrien Bardes, Laurent Najman, and Yann LeCun. Learning and leveraging world models in visual representation learning. *arXiv preprint arXiv:2403.00504*, 2024.

Shivam Grover, Amin Jalali, and Ali Etemad. Segment, shuffle, and stitch: A simple layer for improving time-series representations. In *The Thirty-eighth Annual Conference on Neural Information Processing Systems*, 2024. URL `https://openreview.net/forum?id=zm1LcgRpHm`.

Kai Han, Yunhe Wang, Qi Tian, Jianyuan Guo, Chunjing Xu, and Chang Xu. Ghostnet: More features from cheap operations. In *Proceedings of the IEEE/CVF conference on computer vision and pattern recognition*, pp. 1580–1589, 2020.

Kaiming He, Xinlei Chen, Saining Xie, Yanghao Li, Piotr Dollár, and Ross Girshick. Masked autoencoders are scalable vision learners. In *Proceedings of the IEEE/CVF conference on computer vision and pattern recognition*, pp. 16000–16009, 2022.

Dan Hendrycks and Thomas Dietterich. Benchmarking neural network robustness to common corruptions and perturbations. *Proceedings of the International Conference on Learning Representations*, 2019.

Dan Hendrycks and Kevin Gimpel. Bridging nonlinearities and stochastic regularizers with gaussian error linear units. *arXiv preprint arXiv:1606.08415*, 2016.

Dan Hendrycks, Steven Basart, Norman Mu, Saurav Kadavath, Frank Wang, Evan Dorundo, Rahul Desai, Tyler Zhu, Samyak Parajuli, Mike Guo, et al. The many faces of robustness: A critical analysis of out-of-distribution generalization. In *Proceedings of the IEEE/CVF international conference on computer vision*, pp. 8340–8349, 2021.

Markus Hiller, Krista A. Ehinger, and Tom Drummond. Perceiving longer sequences with bi-directional cross-attention transformers. In *Advances in Neural Information Processing Systems (NeurIPS)*, volume 37, pp. 94097–94129, 2024.

Andrew Howard, Mark Sandler, Grace Chu, Liang-Chieh Chen, Bo Chen, Mingxing Tan, Weijun Wang, Yukun Zhu, Ruoming Pang, Vijay Vasudevan, et al. Searching for mobilenetv3. In *Proceedings of the IEEE/CVF international conference on computer vision*, pp. 1314–1324, 2019.

Andrew G Howard. Mobilenets: Efficient convolutional neural networks for mobile vision applications. *arXiv preprint arXiv:1704.04861*, 2017.

Andrew G. Howard, Menglong Zhu, Bo Chen, Dmitry Kalenichenko, Weijun Wang, Tobias Weyand, Marco Andreetto, and Hartwig Adam. Mobilenets: Efficient convolutional neural networks for mobile vision applications, 2017. URL https://arxiv.org/abs/1704.04861.

Edward J Hu, yelong shen, Phillip Wallis, Zeyuan Allen-Zhu, Yuanzhi Li, Shean Wang, Lu Wang, and Weizhu Chen. LoRA: Low-rank adaptation of large language models. In *International Conference on Learning Representations*, 2022. URL https://openreview.net/forum?id=nZeVKeeFYf9.

Yang Hu, Xiao Wang, Lirong Wu, Huatian Zhang, Stan Z Li, Sheng Wang, and Tianlong Chen. Fm-ts: Flow matching for time series generation. *arXiv preprint arXiv:2411.07506*, 2024.

Sergey Ioffe and Christian Szegedy. Batch normalization: Accelerating deep network training by reducing internal covariate shift, 2015. URL https://arxiv.org/abs/1502.03167.

Andrew Jaegle, Felix Gimeno, Andy Brock, Oriol Vinyals, Andrew Zisserman, and Joao Carreira. Perceiver: General perception with iterative attention. In *International conference on machine learning*, pp. 4651–4664. PMLR, 2021.

Alexander Kirillov, Eric Mintun, Nikhila Ravi, Hanzi Mao, Chloe Rolland, Laura Gustafson, Tete Xiao, Spencer Whitehead, Alexander C. Berg, Wan-Yen Lo, Piotr Dollár, and Ross Girshick. Segment anything. *arXiv:2304.02643*, 2023.

Xuan-May Le, Ling Luo, Uwe Aickelin, and Minh-Tuan Tran. Shapeformer: Shapelet transformer for multivariate time series classification. In *Proceedings of the 30th ACM SIGKDD Conference on Knowledge Discovery and Data Mining*, KDD '24, pp. 1484–1494, New York, NY, USA, 2024. Association for Computing Machinery. doi: 10.1145/3637528.3671862. URL https://doi.org/10.1145/3637528.3671862.

Matthew Leigh, Samuel Klein, François Charton, Tobias Golling, Lukas Heinrich, Michael Kagan, Inês Ochoa, and Margarita Osadchy. Is tokenization needed for masked particle modelling? *arXiv preprint arXiv:2409.12589*, 2024.

Vincent Leroy, Jerome Revaud, Thomas Lucas, and Philippe Weinzaepfel. Win-win: Training high-resolution vision transformers from two windows. In *The Twelfth International Conference on Learning Representations*, 2024. URL https://openreview.net/forum?id=N23A4ybMJr.

Yanyu Li, Geng Yuan, Yang Wen, Ju Hu, Georgios Evangelidis, Sergey Tulyakov, Yanzhi Wang, and Jian Ren. Efficientformer: Vision transformers at mobilenet speed. *Advances in Neural Information Processing Systems*, 35:12934–12949, 2022.

Yanyu Li, Ju Hu, Yang Wen, Georgios Evangelidis, Kamyar Salahi, Yanzhi Wang, Sergey Tulyakov, and Jian Ren. Rethinking vision transformers for mobilenet size and speed. In *Proceedings of the IEEE/CVF International Conference on Computer Vision*, pp. 16889–16900, 2023.

Shilong Liu, Zhaoyang Zeng, Tianhe Ren, Feng Li, Hao Zhang, Jie Yang, Qing Jiang, Chunyuan Li, Jianwei Yang, Hang Su, et al. Grounding dino: Marrying dino with grounded pre-training for open-set object detection. In *European Conference on Computer Vision*, pp. 38–55. Springer, 2025.

Yue Liu, Christos Matsoukas, Fredrik Strand, Hossein Azizpour, and Kevin Smith. Patchdropout: Economizing vision transformers using patch dropout. In *Proceedings of the IEEE/CVF Winter Conference on Applications of Computer Vision*, pp. 3953–3962, 2023.

Zhuang Liu, Hanzi Mao, Chao-Yuan Wu, Christoph Feichtenhofer, Trevor Darrell, and Saining Xie. A convnet for the 2020s. In *Proceedings of the IEEE/CVF conference on computer vision and pattern recognition*, pp. 11976–11986, 2022.

I Loshchilov. Decoupled weight decay regularization. *arXiv preprint arXiv:1711.05101*, 2017.

Sachin Mehta and Mohammad Rastegari. Mobilevit: light-weight, general-purpose, and mobile-friendly vision transformer. *arXiv preprint arXiv:2110.02178*, 2021.

Sachin Mehta and Mohammad Rastegari. Separable self-attention for mobile vision transformers. *arXiv preprint arXiv:2206.02680*, 2022.

Kaouther Messaoud, Matthieu Cord, and Alexandre Alahi. Towards generalizable trajectory prediction using dual-level representation learning and adaptive prompting. *arXiv preprint arXiv:2501.04815*, 2025.

Khan Muhammad, Amin Ullah, Jaime Lloret, Javier Del Ser, and Victor Hugo C de Albuquerque. Deep learning for safe autonomous driving: Current challenges and future directions. *IEEE Transactions on Intelligent Transportation Systems*, 22(7):4316–4336, 2020.

Yuqi Nie, Nam H. Nguyen, Phanwadee Sinthong, and Jayant Kalagnanam. A time series is worth 64 words: Long-term forecasting with transformers. In *International Conference on Learning Representations*, 2023.

Shuaicheng Niu, Jiaxiang Wu, Yifan Zhang, Zhiquan Wen, Yaofo Chen, Peilin Zhao, and Mingkui Tan. Towards stable test-time adaptation in dynamic wild world. In *The Eleventh International Conference on Learning Representations*, 2023. URL `https://openreview.net/forum?id=g2YraF75Tj`.

Soroush Omranpour, Guillaume Rabusseau, and Reihaneh Rabbany. Higher order transformers: Enhancing stock movement prediction on multimodal time-series data. *arXiv preprint arXiv:2412.10540*, 2024.

Maxime Oquab, Timothée Darcet, Théo Moutakanni, Huy V. Vo, Marc Szafraniec, Vasil Khalidov, Pierre Fernandez, Daniel HAZIZA, Francisco Massa, Alaaeldin El-Nouby, Mido Assran, Nicolas Ballas, Wojciech Galuba, Russell Howes, Po-Yao Huang, Shang-Wen Li, Ishan Misra, Michael Rabbat, Vasu Sharma, Gabriel Synnaeve, Hu Xu, Herve Jegou, Julien Mairal, Patrick Labatut, Armand Joulin, and Piotr Bojanowski. DINOv2: Learning robust visual features without supervision. *Transactions on Machine Learning Research*, 2024. ISSN 2835-8856. URL `https://openreview.net/forum?id=a68SUt6zFt`. Featured Certification.

Junting Pan, Adrian Bulat, Fuwen Tan, Xiatian Zhu, Lukasz Dudziak, Hongsheng Li, Georgios Tzimiropoulos, and Brais Martinez. Edgevits: Competing light-weight cnns on mobile devices with vision transformers. In *European Conference on Computer Vision*, pp. 294–311. Springer, 2022.

William Peebles and Saining Xie. Scalable diffusion models with transformers. *arXiv preprint arXiv:2212.09748*, 2022.

Danfeng Qin, Chas Leichner, Manolis Delakis, Marco Fornoni, Shixin Luo, Fan Yang, Weijun Wang, Colby Banbury, Chengxi Ye, Berkin Akin, et al. Mobilenetv4: Universal models for the mobile ecosystem. In *European Conference on Computer Vision*, pp. 78–96. Springer, 2025.

Alec Radford, Jong Wook Kim, Chris Hallacy, Aditya Ramesh, Gabriel Goh, Sandhini Agarwal, Girish Sastry, Amanda Askell, Pamela Mishkin, Jack Clark, Gretchen Krueger, and Ilya Sutskever. Learning transferable visual models from natural language supervision, 2021a. URL `https://arxiv.org/abs/2103.00020`.

Alec Radford, Jong Wook Kim, Chris Hallacy, Aditya Ramesh, Gabriel Goh, Sandhini Agarwal, Girish Sastry, Amanda Askell, Pamela Mishkin, Jack Clark, et al. Learning transferable visual models from natural language supervision. In *International conference on machine learning*, pp. 8748–8763. PMLR, 2021b.

Benjamin Recht, Rebecca Roelofs, Ludwig Schmidt, and Vaishaal Shankar. Do imagenet classifiers generalize to imagenet? In *International conference on machine learning*, pp. 5389–5400. PMLR, 2019.

Tal Ridnik, Emanuel Ben-Baruch, Asaf Noy, and Lihi Zelnik-Manor. Imagenet-21k pretraining for the masses. In *Thirty-fifth Conference on Neural Information Processing Systems Datasets and Benchmarks Track (Round 1)*, 2021. URL `https://openreview.net/forum?id=Zkj_VcZ6ol`.

Esther Rolf, Konstantin Klemmer, Caleb Robinson, and Hannah Kerner. Position: Mission critical – satellite data is a distinct modality in machine learning. In *Proceedings of the 41st International Conference on Machine Learning*, pp. 42691–42706, 2024.

Olga Russakovsky, Jia Deng, Hao Su, Jonathan Krause, Sanjeev Satheesh, Sean Ma, Zhiheng Huang, Andrej Karpathy, Aditya Khosla, Michael Bernstein, et al. Imagenet large scale visual recognition challenge. *International journal of computer vision*, 115:211–252, 2015.

Mark Sandler, Andrew Howard, Menglong Zhu, Andrey Zhmoginov, and Liang-Chieh Chen. Mobilenetv2: Inverted residuals and linear bottlenecks. In *Proceedings of the IEEE conference on computer vision and pattern recognition*, pp. 4510–4520, 2018.

Andreas Peter Steiner, Alexander Kolesnikov, Xiaohua Zhai, Ross Wightman, Jakob Uszkoreit, and Lucas Beyer. How to train your vit? data, augmentation, and regularization in vision transformers. *Transactions on Machine Learning Research*, 2022. ISSN 2835-8856. URL `https://openreview.net/forum?id=4nPswr1KcP`.

Mingxing Tan, Bo Chen, Ruoming Pang, Vijay Vasudevan, Mark Sandler, Andrew Howard, and Quoc V Le. Mnasnet: Platform-aware neural architecture search for mobile. In *Proceedings of the IEEE/CVF conference on computer vision and pattern recognition*, pp. 2820–2828, 2019.

Hugo Thimonier, José Lucas De Melo Costa, Fabrice Popineau, Arpad Rimmel, and Bich-Liên Doan. T-jepa: Augmentation-free self-supervised learning for tabular data. *arXiv preprint arXiv:2410.05016*, 2024.

Hugo Touvron, Matthieu Cord, and Hervé Jégou. Deit iii: Revenge of the vit. In *European conference on computer vision*, pp. 516–533. Springer, 2022.

Lorenzo Vaquero, Yihong Xu, Xavier Alameda-Pineda, Víctor M Brea, and Manuel Mucientes. Lost and found: Overcoming detector failures in online multi-object tracking. In *European Conference on Computer Vision*, pp. 448–466. Springer, 2024.

Pavan Kumar Anasosalu Vasu, James Gabriel, Jeff Zhu, Oncel Tuzel, and Anurag Ranjan. Mobileone: An improved one millisecond mobile backbone. In *Proceedings of the IEEE/CVF conference on computer vision and pattern recognition*, pp. 7907–7917, 2023a.

Pavan Kumar Anasosalu Vasu, James Gabriel, Jeff Zhu, Oncel Tuzel, and Anurag Ranjan. Fastvit: A fast hybrid vision transformer using structural reparameterization. In *Proceedings of the IEEE/CVF International Conference on Computer Vision*, 2023b.

Shashanka Venkataramanan, Valentinos Pariza, Mohammadreza Salehi, Lukas Knobel, Spyros Gidaris, Elias Ramzi, Andrei Bursuc, and Yuki M. Asano. Franca: Nested matryoshka clustering for scalable visual representation learning, 2025. URL `https://arxiv.org/abs/2507.14137`.

Shuzhe Wang, Vincent Leroy, Yohann Cabon, Boris Chidlovskii, and Jerome Revaud. Dust3r: Geometric 3d vision made easy. In *Proceedings of the IEEE/CVF Conference on Computer Vision and Pattern Recognition (CVPR)*, pp. 20697–20709, June 2024.

Yibing Wei, Abhinav Gupta, and Pedro Morgado. Towards latent masked image modeling for self-supervised visual representation learning. In *European Conference on Computer Vision*, pp. 1–17. Springer, 2025.

Ross Wightman. Pytorch image models. `https://github.com/rwightman/pytorch-image-models`, 2019.

Sanghyun Woo, Shoubhik Debnath, Ronghang Hu, Xinlei Chen, Zhuang Liu, In So Kweon, and Saining Xie. Convnext v2: Co-designing and scaling convnets with masked autoencoders. In *Proceedings of the IEEE/CVF Conference on Computer Vision and Pattern Recognition*, pp. 16133–16142, 2023.

Seokju Yun and Youngmin Ro. Shvit: Single-head vision transformer with memory efficient macro design. In *Proceedings of the IEEE/CVF Conference on Computer Vision and Pattern Recognition (CVPR)*, pp. 5756–5767, 2024.

George Zerveas, Srideepika Jayaraman, Dhaval Patel, Anuradha Bhamidipaty, and Carsten Eickhoff. A transformer-based framework for multivariate time series representation learning. In *Proceedings of the 27th ACM SIGKDD Conference on Knowledge Discovery &; Data Mining*, KDD '21, pp. 2114–2124, 2021.

Bowen Zhang, Zhi Tian, Quan Tang, Xiangxiang Chu, Xiaolin Wei, Chunhua Shen, et al. Segvit: Semantic segmentation with plain vision transformers. *Advances in Neural Information Processing Systems*, 35:4971–4982, 2022.

A Appendix

A.1 Impact Statement

This work presents new designs and empirical results for deep network architectures for more accurate and computationally efficient modeling applied to visual recognition and time series processing. This general topic does not have more specific societal consequences aside from those inherited, good or bad, from the adoption of machine learning.

A.2 Compute-efficient Architecture Descriptions

❶ EfficientViT Cai et al. (2023) is a hierarchical architecture with four stages and one head. Stages 1 and 2 consist of MBConv layers Sandler et al. (2018). Stages 3 and 4 consist of MBConv sublayers and their novel EfficientViT sublayer, consisting of an efficient attention module and an FFN+DWConv module Howard (2017). Their attention module creates queries, keys, and values of three scales via three DWConvs, and then each set of queries, keys, and values undergoes efficient linear attention. Finally, the head receives outputs from Stages 2, 3, and 4, and applies a final MBConv. EfficientViT variants differ in stage depths and widths, as well as head width.

❷ SHViT Yun & Ro (2024) is a hierarchical architecture with three stages. Stage 1 consists of a DWConv+BatchNorm sublayer and an FFN sublayer. Stages 2 and 3 incorporate their novel single-headed self-attention (SHSA) sublayer between the stage 1 sublayers. SHSA consists of performing single-headed self-attention on a fraction of dimensions ($1/4.67$ ratio); the other dimensions pass straight through, further reducing cost. Both FFN and SHSA sublayers also replace linear layers with DWConv. SHViT variants differ in stage depths and widths.

❸ MobileNetV4 Qin et al. (2025) variants use their FusedIB, ExtraDW, and Mobile MQA (multi-query attention) modules along with MBConv, ConvNext-Like Liu et al. (2022), and FFN modules. Variants differ in stage depths and widths, the number of stages, and stage architectures built with a combination of the listed modules.

A.3 Experimental Details

A.3.1 ImageNet-1K and -21K Hyperparameters

We pick these recipes based on findings in the literature—such as Touvron et al. (2022), Fuller et al. (2024), Beyer et al. (2022), Dehghani et al. (2024), and Steiner et al. (2022)—and past experience indicating that these recipes would result in strong models.

ImageNet-1K training recipe: 128×128 px images, 400 epochs, 1024 batch size, PyTorch's AdamW optimizer with a 0.05 weight decay, 1.0 clip grad norm, `deit3-base-patch16-224.fb-in22k-ft-in1k` teacher Touvron et al. (2022) given 224×224 px images using Wightman (2019)'s implementation, KL divergence loss between student and teacher logits Beyer et al. (2022), linear learning rate warmup for 10% of steps to $\{1\text{e}{-3}, 3\text{e}{-3}\}$ and cooldown using a cosine decay schedule to $1\text{e}{-5}$, mixup $\alpha = 0.8$, cutmix $\alpha = 1$, and 3-Augment data augmentation Touvron et al. (2022). Then we continue training at 224×224 px images, 20 epochs, 512 batch size, PyTorch's AdamW optimizer with a 0.1 weight decay, 1.0 clip grad norm, `deit3-large-patch16-224.fb-in22k-ft-in1k` teacher Touvron et al. (2022) given 224×224 px images using Wightman (2019)'s implementation, KL divergence loss between student and teacher logits Beyer et al. (2022), linear learning rate warmup for 25% of steps to $5\text{e}{-5}$ and cooldown using a cosine decay schedule to $1\text{e}{-5}$, mixup $\alpha = 0.8$, cutmix $\alpha = 1$, and AutoAugment ("rand-m9-mstd0.5-inc1") data augmentation Cubuk et al. (2018) following DEIT III's Touvron et al. (2022) high-res finetuning recipe.

ImageNet-21K training recipe: 224×224 px images, 50 epochs, 1024 batch size, PyTorch's AdamW optimizer with a 0.02 weight decay, 1.0 clip grad norm, cross-entropy loss, linear learning rate warmup for 10% of steps to $3\text{e}{-3}$ and cooldown using a cosine decay schedule to $1\text{e}{-5}$, mixup $\alpha = 0.8$, cutmix $\alpha = 0$, and 3-Augment data augmentation Touvron et al. (2022). To speed up training, we also employ a token dropping strategy starting at 90%, linearly decreasing to 10%.

A.3.2 Time Series Experiments

We adopt the PatchTST Nie et al. (2023) architecture for our time series experiments. PatchTST is a patch-based transformer architecture for time series processing. The method splits a univariate time series into patches processed as they are in ViTs for classification, aside from position encoding (2D vs. 1D). For multivariate series, each channel is processed *independently* using the shared transformer backbone, with the final-layer `CLS` tokens from each channel concatenated before classification. We extend this shared backbone with registers (PatchTST+Registers) and Jumbo (PatchTST+Jumbo).

We closely follow the PatchTST training recipe for our experiments, making minor adjustments based on prior experience to enhance performance. This method remains competitive with recent transformer-based benchmarks for time series classification Zerveas et al. (2021); Grover et al. (2024); Le et al. (2024). Apart from variations in time series length, all experiments use the same hyperparameters and methodology.

PatchTST Hyperparameters: The model comprises 3 encoder layers, each with 16 attention heads and a token width of $D = 128$. The transformer FFN includes two linear layers with a GELU activation Hendrycks & Gimpel (2016); the first expands the hidden dimension to 256, while the second projects it back to 128. For PatchTST+Jumbo, we use $J = 4$. For PatchTST+Registers, R is calculated according to Appendix A.3.3.

Time Series training recipe: We perform a hyperparameter sweep over the Cartesian product of learning rates $\{$3e-3, 1e-3, 3e-4, 1e$-4\}$ and dropout rates $\{0.0, 0.1, 0.2\}$. Each configuration uses either 8 or 42 equally sized patches of maximum possible length, with end-padding applied as needed. The stride length is set to half the patch length. Unless stated otherwise, all experiments follow the same setup: 100 epochs, 256 batch size, PyTorch's AdamW optimizer with a 0.02 weight decay, cross-entropy loss, and a linear learning rate warmup for the first 10% of steps, followed by a cooldown using cosine decay to 1e-8. For large datasets, we reduce the number of epochs to ensure efficient processing within a reasonable time frame; specifically, we train datasets $\{$Sleep, Tiselac, FaceDetection$\}$ for 20 epochs.

Each dataset from the UEA and UCR archives includes a prescribed validation set. We create a new 50/50 test/validation split from each of these original validation sets, selecting the best run based on validation performance. All reported results are from the *test* set.

The 20 datasets were selected in decreasing order of their number of training examples; datasets with either (i) fewer than 42 total timesteps or (ii) significant data preparation issues were excluded.

A.3.3 FLOP Details

To ensure a fair comparison, we configure PatchTST+Registers and PatchTST+Jumbo to have approximately equal per-layer FLOPs by selecting the number of registers R in the former and the Jumbo multiplier J in the latter accordingly. Additionally, we apply average pooling to the J split segments of the Jumbo token to prevent a significant increase in the number of learnable parameters of the classification head. This pooling produces a token of width D per channel before concatenation, effectively serving the same role as a `CLS` token. The detailed per-layer FLOP calculation is provided by the proposition below.

Proposition 1. Let P be the total number of local patch tokens, R the number of register tokens, D the width, and J the Jumbo multiplier. Given an FFN hidden dimension of $2D$, and otherwise fixed parameters, a Register architecture with R registers has the same per-layer FLOP count as a Jumbo architecture with multiplier J if and only if

$$R = -(2D + P) + \sqrt{(2D + P)^2 + (1 + 2D)J^2 + 2(D + P)J}$$

Proof. Let F denote the FLOP count. Given a sequence length of n tokens, each of width d, the FLOP contributions from the MHSA and FFN sublayers in a single transformer layer with a FFN hidden dimension of ld are given by

$$F_{\text{MHSA}} = 4nd^2 + 2n^2d \quad \text{and} \quad F_{\text{FFN}} = l^2nd^2 = 4nd^2$$

where we fix $l = 2$. For the Register architecture, $n = P + R$ and $d = D$ for both the MHSA and the FFN contributions. For the Jumbo architecture, $n = P + J$ and $d = D$ for MHSA. The FFN contribution is split; local patch tokens contribute with $n = P, d = D$ while the dedicated Jumbo FFN has $n = 1, d = JD$. From summing the contributions, it follows that

$$F_{\text{Reg}} = 4(P+R)D^2 + 2(P+R)^2 D + 4(P+R)D^2$$
$$F_{\text{Jumbo}} = 4(P+J)D^2 + 2(P+J)^2 D + 4PD^2 + 4J^2 D^2$$

Equating $F_{\text{Reg}} = F_{\text{Jumbo}}$ and solving for R gives the stated result. □

In our time series experiments, we compute R, rounding to the nearest integer, to match the per-layer FLOP count of a Jumbo architecture with multiplier J as closely as possible.

A.4 Detailed ImageNet-1K Results

Table 6: All final results obtained on 224×224 px images (%).

Architecture	Size	Throughput	ImageNet-Val		ImageNet-ReaL		ImageNet-v2		ImageNet-R		ImageNet-HR	
		224^2 px	Top-1	Top-5	Top-1	Top-5	Top-1	Top-5	Top-1	Top-5	Top-1	Top-5
ViT+Jumbo	D=96, J=6	43.7K	69.0	88.5	76.6	92.3	56.0	79.0	23.5	37.1	77.9	92.6
	D=128, J=6	31.3K	74.0	91.5	81.3	94.7	61.4	83.4	27.4	42.6	83.2	95.0
	D=192, J=6	20.4K	78.4	94.0	84.8	96.3	66.2	87.0	31.7	47.3	86.8	96.2
	D=384, J=6	7.6K	82.7	96.4	88.0	97.8	72.4	90.6	39.0	55.6	90.9	98.3
ViT+Registers	D=128, R=16	25.5K	61.0	84.1	68.9	88.9	49.1	74.1	18.7	32.4	69.7	88.9
	D=192, R=16	16.7K	74.5	92.3	82.3	95.4	62.5	84.7	28.2	43.5	83.7	95.6
	D=384, R=16	6.6K	81.9	96.0	87.4	97.7	71.4	90.2	38.0	53.8	90.0	98.0
MobileNetV4	conv-small	33.7K	65.6	86.2	73.3	90.7	52.5	75.5	22.3	37.5	75.7	91.3
	conv-medium	11.2K	74.9	92.6	82.4	95.5	63.1	84.8	29.4	45.9	84.7	95.8
	hybrid-medium	8.8K	78.1	94.3	85.0	96.7	67.0	87.5	33.0	49.4	87.2	96.8
SHViT	S1	42.1K	67.9	88.2	75.7	92.2	54.7	78.2	23.1	38.0	77.6	92.7
	S2	34.5K	71.0	90.0	78.6	93.6	58.4	80.5	25.6	41.1	80.9	93.9
	S3	23.7K	74.3	92.0	81.6	95.0	61.8	83.5	28.3	43.9	84.0	95.4
EfficientViT	B0	25.2K	66.3	86.5	73.9	90.7	53.6	76.3	22.2	36.7	75.8	91.0
	B1	9.8K	76.9	93.5	83.7	96.2	64.5	85.9	31.3	47.2	85.8	96.4

Table 7: ViT+Registers results, obtained on 128×128 px images (%).

Patch	Num.	Learning	Throughput	ImageNet-Val		ImageNet-ReaL		ImageNet-v2		ImageNet-R		ImageNet-HR	
Width	Registers	Rate	imgs/s	Top-1	Top-5	Top-1	Top-5	Top-1	Top-5	Top-1	Top-5	Top-1	Top-5
128	16	3e−3	107.0K	53.6	78.5	60.8	83.6	42.4	67.8	15.9	28.6	61.9	83.4
	16	1e−3		51.9	76.8	59.0	81.8	40.8	65.4	13.7	24.9	60.5	82.6
192	8	3e−3	65.7K	68.5	88.8	76.1	92.6	55.7	78.8	24.9	39.4	77.8	92.2
	16	3e−3	59.9K	68.8	88.9	76.6	92.6	55.9	79.4	24.8	38.9	78.5	92.5
	16	1e−3		66.1	87.2	74.0	91.2	54.2	77.0	22.9	36.2	75.4	91.6
384	8	3e−3	24.6K	77.8	93.9	84.3	96.2	65.8	86.3	33.3	48.6	86.8	96.5
	16	3e−3	21.8K	78.1	94.0	84.5	96.3	66.1	86.6	33.3	48.6	86.6	96.5
	16	1e−3		78.2	94.1	84.5	96.3	66.4	86.6	33.5	48.4	87.2	96.6

Table 8: ViT+Jumbo results, obtained on 128×128 px images (%).

Patch	Learning	Throughput	ImageNet-Val		ImageNet-ReaL		ImageNet-v2		ImageNet-R		ImageNet-HR	
Width	Rate	imgs/s	Top-1	Top-5	Top-1	Top-5	Top-1	Top-5	Top-1	Top-5	Top-1	Top-5
96	3e−3	136.0K	62.4	83.7	69.6	88.1	49.3	72.9	20.1	33.5	71.4	89.1
	1e−3		60.8	82.9	68.0	87.3	48.3	71.8	18.9	31.6	70.3	87.6
128	3e−3	103.1K	67.7	87.5	75.0	91.2	54.3	77.6	24.1	37.5	76.6	92.1
	1e−3		68.4	87.9	75.6	91.6	55.2	78.0	23.8	37.6	77.0	92.1
192	3e−3	57.3K	73.3	91.2	80.2	94.1	60.5	82.1	28.0	42.2	82.7	94.6
	1e−3		73.5	91.3	80.3	94.1	60.5	81.8	27.8	42.2	82.8	94.4
384	3e−3	20.4K	79.3	94.4	85.3	96.5	67.3	87.0	34.3	49.5	88.3	96.8
	1e−3		79.3	94.5	85.1	96.6	66.7	86.7	33.4	48.4	87.7	96.6

Table 9: MobileNetV4 results, obtained on 128×128 px images (%).

Size	Learning Rate	Throughput imgs/s	ImageNet-Val		ImageNet-ReaL		ImageNet-v2		ImageNet-R		ImageNet-HR	
			Top-1	Top-5	Top-1	Top-5	Top-1	Top-5	Top-1	Top-5	Top-1	Top-5
conv-small	3e−3	142.7K	62.1	83.6	69.2	88.1	49.1	72.8	20.4	34.3	71.8	89.4
	1e−3		60.0	82.0	67.2	86.7	47.6	71.4	18.9	32.2	69.8	87.7
conv-medium	3e−3	53.8K	73.3	91.5	80.5	94.6	60.6	82.9	27.7	42.8	83.2	95.3
	1e−3		72.2	90.7	79.4	94.0	59.5	81.7	27.0	42.0	82.0	94.6
hybrid-medium	3e−3	43.5K	74.9	92.4	81.8	95.3	62.4	84.0	29.5	44.8	84.4	95.5
	1e−3		75.2	92.5	82.0	95.3	63.0	84.5	29.1	44.5	84.2	95.4

Table 10: SHViT results, obtained on 128×128 px images (%).

Size	Learning Rate	Throughput imgs/s	ImageNet-Val		ImageNet-ReaL		ImageNet-v2		ImageNet-R		ImageNet-HR	
			Top-1	Top-5	Top-1	Top-5	Top-1	Top-5	Top-1	Top-5	Top-1	Top-5
S1	3e−3	81.0K	63.5	84.9	70.9	89.1	50.8	74.5	22.2	35.7	73.7	90.0
	1e−3		63.5	85.1	71.0	89.3	50.9	74.4	21.3	34.7	72.9	90.5
S1	3e−3	76.1K	66.6	87.0	73.9	90.8	54.0	76.6	23.9	38.0	76.1	91.7
	1e−3		66.7	87.0	73.8	90.8	53.7	76.8	24.0	37.8	76.7	92.0
S3	3e−3	73.8K	70.5	89.8	77.7	93.1	58.1	80.4	26.6	41.0	80.4	93.8
	1e−3		71.2	90.0	78.3	93.3	58.6	80.7	26.7	40.7	80.7	93.9

Table 11: EfficientViT results, obtained on 128×128 px images (%).

Size	Learning Rate	Throughput imgs/s	ImageNet-Val		ImageNet-ReaL		ImageNet-v2		ImageNet-R		ImageNet-HR	
			Top-1	Top-5	Top-1	Top-5	Top-1	Top-5	Top-1	Top-5	Top-1	Top-5
B0	3e−3	98.6K	59.5	81.9	66.8	86.7	46.8	70.3	18.6	32.0	69.3	87.6
	1e−3		60.8	82.6	68.0	87.2	48.3	71.6	19.3	32.6	70.4	87.7
B1	3e−3	38.7K	71.8	90.7	79.2	94.0	59.7	81.8	27.4	42.2	81.5	94.4
	1e−3		72.8	91.0	79.8	94.2	60.4	81.9	27.1	42.3	82.5	94.8

Table 12: ViT+Jumbo ablation results, obtained on 128×128 px images (%).

Patch Width	Jumbo Multiplier	Inner FFN Multiplier	Throughput 128^2 px	Throughput 224^2 px	ImageNet-Val		ImageNet-ReaL		ImageNet-v2		ImageNet-HR		ImageNet-R	
					Top-1	Top-5	Top-1	Top-5	Top-1	Top-5	Top-1	Top-5	Top-1	Top-5
192	2	2	71.6K	21.6K	70.0	89.6	77.5	93.1	57.3	80.0	26.1	40.9	79.3	93.2
		4	69.6K	21.5K	70.4	89.6	77.8	93.1	57.3	79.8	25.5	39.6	79.7	93.3
	4	1	69.6K	21.3K	71.5	90.4	78.8	93.7	59.2	81.3	26.9	41.7	80.8	93.7
		2	68.1K	21.2K	70.6	89.6	77.6	93.0	57.7	79.8	25.9	40.3	80.4	93.5
		4	64.9K	20.8K	72.2	90.6	79.2	93.6	59.3	81.1	26.6	41.2	81.8	94.1
	6	1	65.3K	20.9K	72.1	90.5	79.2	93.7	58.9	81.1	26.4	41.1	80.8	94.2
		2	63.5K	20.6K	71.8	90.2	78.7	93.3	58.2	80.6	25.8	39.8	80.7	93.6
		4	56.5K	19.9K	73.0	90.7	79.6	93.7	59.4	81.2	26.8	41.3	82.3	93.9
384	2	2	27.2K	8.7K	77.0	93.5	83.6	96.0	64.6	85.8	31.9	47.9	85.8	96.4
		4	26.1K	8.6K	78.1	94.0	84.4	96.3	65.9	86.1	32.8	48.7	86.1	96.4
	4	1	26.1K	8.6K	77.3	93.6	83.7	96.0	64.9	85.8	32.1	47.8	86.5	96.2
		2	24.5K	8.5K	77.9	93.9	84.0	96.3	65.7	85.9	32.7	48.6	86.7	96.2
		4	23.6K	8.3K	77.9	93.8	84.0	96.2	65.7	85.8	32.4	48.0	86.2	96.2
	6	1	23.9K	8.4K	77.6	93.6	84.0	96.1	65.8	85.8	32.1	47.9	86.7	96.2
		2	22.9K	8.2K	77.8	93.6	83.8	96.0	65.0	85.3	32.2	47.5	86.6	96.0
		4	19.5K	7.8K	78.3	93.8	84.2	96.1	66.1	86.0	32.9	48.6	87.0	96.3

A.5 Detailed Timeseries Results

Table 13: Univariate time series classification results (%). “Best” refers to the best run of our 12-run hyperparameter sweep and “Avg” refers to the average over the sweep.

		PatchTST/8	PatchTST/8 +Registers	PatchTST/8 +Jumbo	PatchTST/42	PatchTST/42 +Registers	PatchTST/42 +Jumbo
Sleep	Best	70.9	70.7	73.3	70.5	70.6	70.3
	Avg	67.5	67.7	68.3	67.2	67.1	67.6
InsectSound	Best	82.8	83.3	83.7	85.8	84.4	85.6
	Avg	76.7	76.0	78.7	78.7	78.7	79.7
FruitFlies	Best	92.2	90.9	92.2	95.2	95.0	95.1
	Avg	88.4	88.4	89.4	93.1	92.9	93.9
RightWhaleCalls	Best	94.3	93.8	95.1	96.7	97.0	96.1
	Avg	92.8	93.5	94.2	94.0	94.8	95.1
FaultDetectionA	Best	98.0	97.7	98.1	99.6	99.8	99.8
	Avg	94.6	95.2	97.2	99.2	99.2	99.5
ElectricDevices	Best	89.0	88.8	90.1	92.4	92.4	92.5
	Avg	81.6	83.2	84.0	85.1	85.2	88.1
Crop	Best	80.9	81.2	82.0	81.2	80.6	82.2
	Avg	69.4	70.9	72.0	68.7	68.3	68.7
FordB	Best	98.8	97.3	97.7	97.7	96.5	96.5
	Avg	95.4	96.0	96.6	95.7	94.9	94.8
FordA	Best	97.3	98.0	97.7	97.1	97.1	97.5
	Avg	96.1	96.6	97.2	95.5	95.7	96.0
MelbournePedestrian	Best	92.1	91.5	91.0	90.4	91.0	93.1
	Avg	81.8	82.8	83.9	83.5	83.8	84.9

Table 14: Multivariate time series classification results (%). “Best” refers to the best run of our 12-run hyperparameter sweep and “Avg” refers to the average over the sweep.

		PatchTST/8	PatchTST/8 +Registers	PatchTST/8 +Jumbo	PatchTST/42	PatchTST/42 +Registers	PatchTST/42 +Jumbo
Tiselac	Best	96.6	96.9	97.2	96.4	96.4	96.7
	Avg	86.9	87.8	90.1	84.7	85.0	87.9
WalkingSittingStanding	Best	96.0	96.0	96.5	98.0	97.6	97.6
	Avg	91.7	89.8	93.5	93.9	93.9	94.5
SpokenArabicDigits	Best	99.9	99.7	99.9	99.7	99.9	99.9
	Avg	99.5	99.6	99.6	99.6	99.5	99.7
FaceDetection	Best	87.8	88.1	87.5	86.8	86.6	84.8
	Avg	78.9	80.9	80.0	77.4	77.4	78.8
PhonemeSpectra	Best	56.3	57.1	59.1	57.6	60.3	58.9
	Avg	38.2	38.7	46.5	42.9	44.5	47.7
LSST	Best	78.7	79.5	79.9	74.6	75.7	79.9
	Avg	69.3	69.4	71.2	61.4	61.4	67.3
UWaveGestureLibrary	Best	92.7	88.5	87.5	94.8	99.0	94.8
	Avg	76.8	79.9	83.4	81.3	83.5	85.4
CharacterTrajectories	Best	99.0	98.0	99.6	98.7	99.3	98.4
	Avg	93.6	94.2	96.6	96.6	95.2	97.0
AsphaltPavementTypeCoordinates	Best	72.3	77.7	81.1	89.5	88.5	89.5
	Avg	72.7	75.8	77.0	81.2	82.1	83.7
MotorImagery	Best	87.5	83.3	77.1	79.2	66.7	87.5
	Avg	84.9	83.3	83.2	73.6	74.0	81.9

A.6 Attention Maps

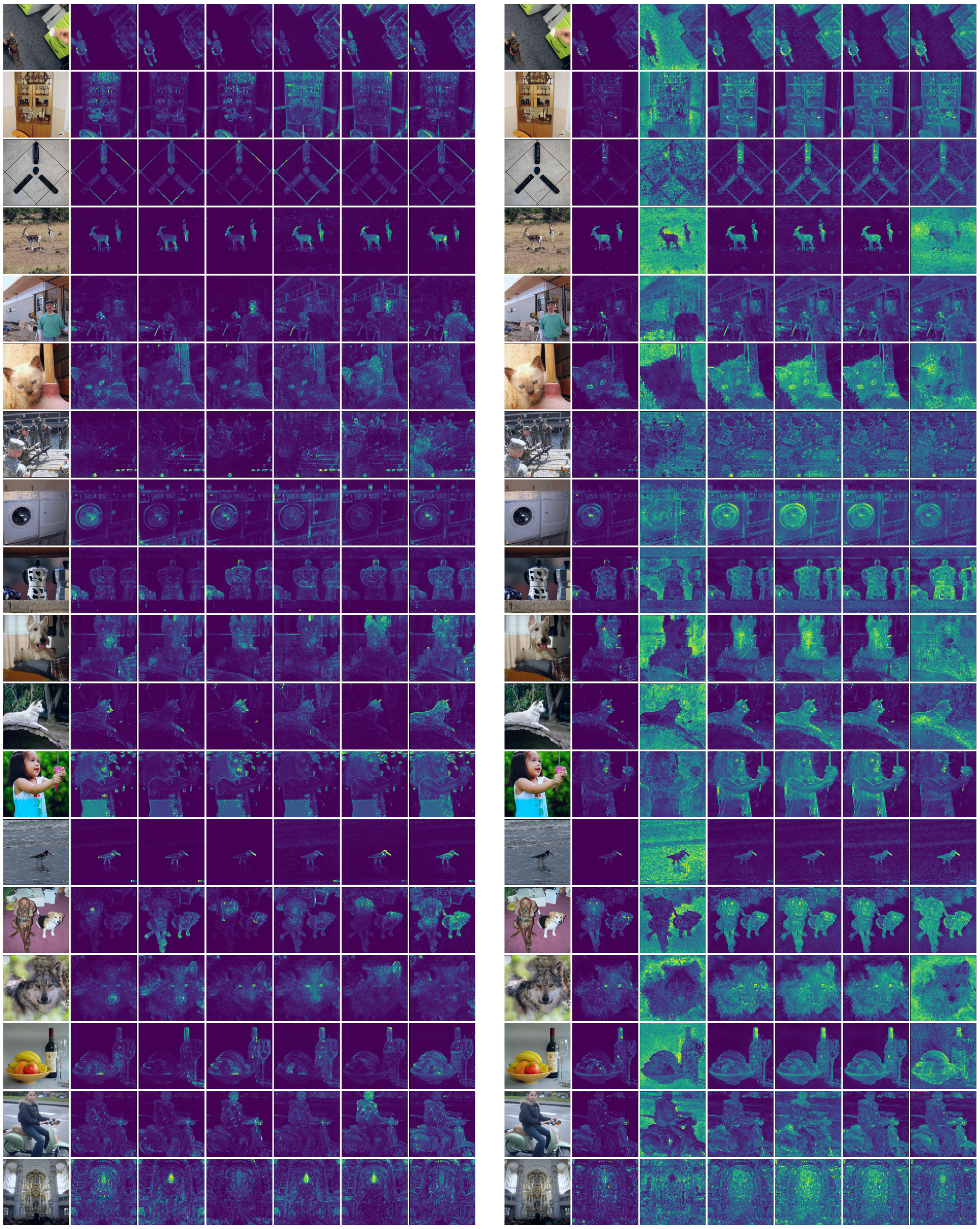

(a) Attention maps of the Jumbo token split into 6 smaller global tokens. Like ViT+Registers, ViT+Jumbo learns relatively artifact-free attention maps (as compared with the attention maps in Darcet et al. (2024)).

(b) Attention maps of the `CLS` and the first five register tokens.